Solar RRL
www.solar-rrl.com

Hydrogenation Mechanisms of Poly-Si/SiO_x Passivating Contacts by Different Capping Layers

Thien N. Truong, Di Yan, Wenhao Chen, Mike Tebyetekerwa, Matthew Young, Mowafak Al-Jassim, Andres Cuevas, Daniel Macdonald, and Hieu T. Nguyen**

Herein, posttreatment techniques of phosphorus-doped poly-Si/SiO_x passivating contacts, including forming gas annealing (FGA), atomic layer deposition (ALD) of hydrogenated aluminum oxide (AlO_x:H), and plasma-enhanced chemical vapor deposition (PECVD) of hydrogenated silicon nitride (SiN_x:H), are investigated and compared in terms of their application to silicon solar cells. A simple FGA posttreatment produces a significant increase in the implied open circuit voltage (iV_{oc}) and the effective minority-carrier lifetime (τ_{eff}) of high-resistivity crystalline Si (c-Si) samples, whereas low-resistivity samples show a minimal change. Treatment by means of AlO_x:H and/or SiN_x:H followed by postdeposition FGA results in a universal increase in τ_{eff} and iV_{oc} for all substrate resistivities (as high as 12.5 ms and 728 mV for 100 Ω cm and 5.4 ms and 727 mV for 2 Ω cm n-type c-Si substrates). In addition, both the FGA and AlO_x:H + FGA techniques can inject sufficient hydrogen into the samples to passivate defects at the SiO_x/c-Si and poly-Si/SiO_x interfaces. However, this hydrogen concentration is insufficient to neutralize both the nonradiative defects inside the poly-Si films and dangling bonds associated with the amorphous Si phase present in them. The hydrogen injected by the SiN_x:H + FGA technique can passivate both the interfaces and the defects and dangling bonds within the poly-Si film. These results are confirmed by low-temperature photoluminescence spectroscopy, Fourier transform infrared spectroscopy, and dynamic secondary-ion mass spectrometry measurements.

Beyond the passivated emitter and rear cell (PERC) crystalline silicon (c-Si) technology, with potential commercial cell conversion efficiencies in the range of 21–24%,[1–3] c-Si solar cells incorporating poly-Si/SiO_x passivating contacts have attracted significant interest as one of the most promising pathways to overcome the efficiency limits of the PERC technology. A laboratory-scale efficiency of 26.1% has been demonstrated on a poly-Si/SiO_x interdigitated back contact (IBC) cell structure,[4] and several researchers have reported cell efficiencies higher than 24% featuring poly-Si/SiO_x passivating contacts.[5–7]

In general, poly-Si films contain a high density of defects, which may affect the passivating-contact performance and thus the conversion efficiency of solar cells. This stems from the fact that poly-Si films, formed by recrystallizing amorphous Si (a-Si) films via a high-temperature processing step, often contain both amorphous and crystalline phases.[8,9] In the a-Si phase, each Si atom is surrounded by four other Si atoms whose bonds are stretched, twisted, or broken (known as dangling bonds). These bonds then create energy levels inside the material bandgap and are responsible for Shockley–Read–Hall (SRH) carrier recombination, even if neither impurities nor extended crystal defects are present in the material.[10–12] One way to overcome this SRH recombination is to neutralize each defective bond inside the films with the addition of a hydrogen atom, that is, by performing a hydrogenation step after the formation of the poly-Si film.

Hydrogenation treatments in c-Si solar cell technology are often performed via forming gas annealing (FGA) of samples in a mixture of H_2 and inert gas,[6,13,14] by annealing the samples without any capping layers in a mixture of water vapor and N_2,[15] or by depositing hydrogen-rich capping layers such as AlO_x:H[16–20] or SiN_x:H[21–23] and annealing them in N_2 or FGA. Previously, we have noticed that in the case of low-resistivity substrates (1 Ω cm), FGA of poly-Si/SiO_x passivating contacts resulted in little performance improvement, whereas others have reported a noticeable improvement.[6,9,13,24] However, when capping

T. N. Truong, Dr. D. Yan, W. Chen, M. Tebyetekerwa, Prof. A. Cuevas, Prof. D. Macdonald, Dr. H. T. Nguyen
Research School of Electrical
Energy and Materials Engineering
The Australian National University
Canberra, ACT 2601, Australia
E-mail: thien.truong@anu.edu.au; hieu.nguyen@anu.edu.au

The ORCID identification number(s) for the author(s) of this article can be found under https://doi.org/10.1002/solr.201900476.

DOI: 10.1002/solr.201900476

W. Chen
Institute of Photovoltaics
Nanchang University
Nanchang 330031, China

M. Young, Dr. M. Al-Jassim
National Center for Photovoltaics
National Renewable Energy Laboratory
Golden, CO 80401, USA

layers and postdeposition annealing treatments are used, the passivating-contact performance improves significantly, as reported by many groups.[9,24–26] It has been shown that, without postdeposition annealing, there is no passivation improvement,[9,24] and also that either annealing in N_2 or FGA shows the same performance.[24]

This communication tries to elucidate the underlying mechanisms of posttreatments of phosphorus-doped poly-Si/SiO_x passivating contacts by different methods, including AlO_x:H and/or SiN_x:H films followed by FGA, and FGA alone. We first study the optoelectronic properties of passivating-contact samples before and after the posttreatments by FGA alone and AlO_x:H capping films followed by FGA. We then track the evolution of these properties after another subsequent hydrogenation process by SiN_x:H capping films followed by FGA to differentiate the mechanisms among the various posttreatment processes.

First, we investigated the effects of FGA on the performance of phosphorus-doped poly-Si/SiO_x passivating contacts with different substrate resistivities. **Figure 1** shows τ_{eff} and iV_{oc} of samples after the different processing steps described in **Figure 2**, for both thermal (A) and plasma (B) ALD AlO_x:H + FGA processes to demonstrate their similar improvement. All samples after the phosphorus diffusion showed good initial passivation qualities (τ_{eff} ≈1.5 ms for 2 Ω cm wafers and ≈3.5–5.5 ms for 100 Ω cm wafers, iV_{oc} ≈685–700 mV). Some of the phosphorus-doped poly-Si/SiO_x samples were then annealed in forming gas at 400 °C for 30 min without any capping layer. The samples with a high resistivity (100 Ω cm) showed a dramatic increment in τ_{eff} and iV_{oc} values after the annealing ($\Delta\tau_{eff} = 6$ ms and $\Delta iV_{oc} = 28$ mV), whereas on low-resistivity samples (2 Ω cm), the change was minimal. The other samples, annealed in forming gas in the presence of an AlO_x:H capping layer, showed a significant increment in τ_{eff} and iV_{oc} values ($\tau_{eff} > 4$ ms for 2 Ω cm wafers and $\Omega_{eff} > 10$ ms for 100 Ω cm wafers, $iV_{oc} > 725$ mV) regardless of the initial conditions.

Figure 3A presents the PL spectra captured from the poly-Si/SiO_x/c-Si sample at 80 K using the 405 nm excitation laser after various processing steps: as diffused and subsequently annealed in forming gas with and without the AlO_x:H capping layer. In all cases, the spectra are nearly identical. There is a sharp peak at ≈1125 nm attributed to the band–band emission from the c-Si substrate[27–29] and a broad peak in the range 1300–1500 nm attributed to the radiative defects inside the poly-Si films, as reported by Nguyen et al.[29] In contrast, it is known that the poly-Si films contain both amorphous and crystalline phases, and the hydrogenated a-Si (a-Si:H) phase will emit a distinct peak located at ≈950 nm.[9] Surprisingly, there is no PL peak from the a-Si:H phase after the AlO_x:H deposition and subsequent FGA (Figure 3A), albeit there being a big improvement in the passivation quality (Figure 1). These results demonstrate that the 40 nm AlO_x:H film had injected some amount of atomic hydrogen into the sample, which sufficiently passivated defects at the SiO_x/c-Si or poly-Si/SiO_x interfaces. However, the hydrogen had not neutralized the nonradiative defects inside

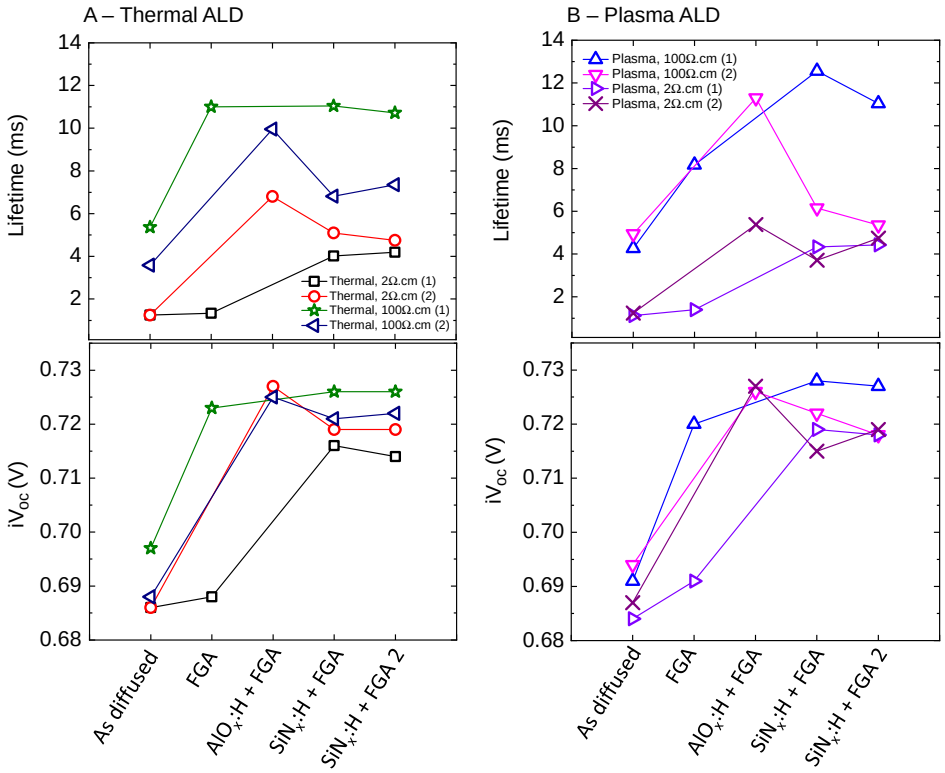

Figure 1. Implied open circuit voltage iV_{oc} and minority carrier lifetime τ_{eff} from samples before and after various hydrogenation methods: FGA alone and A) thermal or B) plasma-assisted AlO_x:H or SiN_x:H followed by FGA. τ_{eff} and iV_{oc} are measured at a minority carrier density of 1×10^{15} cm^{-3} and 1-sun intensity, respectively. The number (1) in the legend denotes samples treated with FGA alone and the number (2) denotes samples treated with AlO_x:H + FGA. The passivation improvement was observed for both plasma and thermal AlO_x:H + FGA.

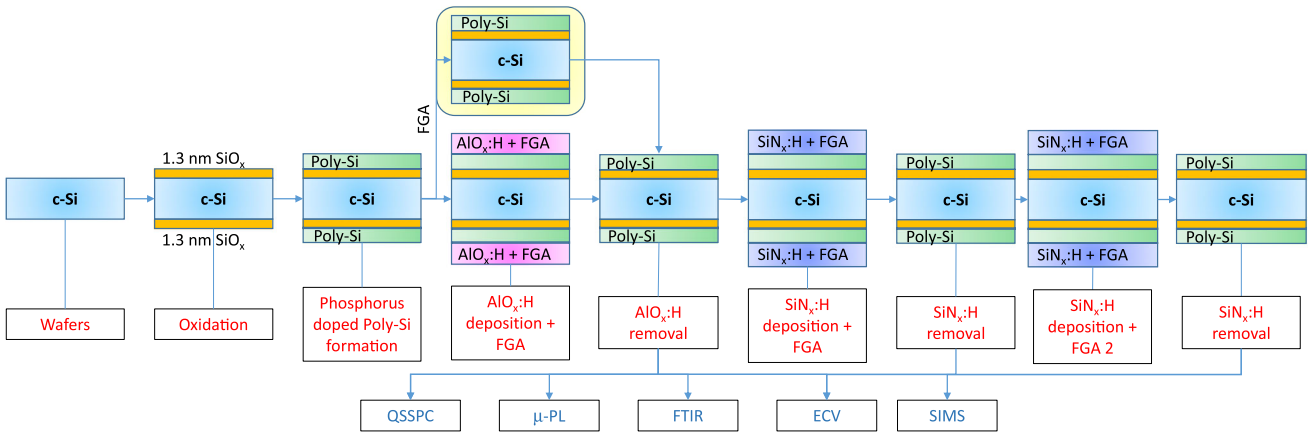

Figure 2. Schematic of the experimental processes.

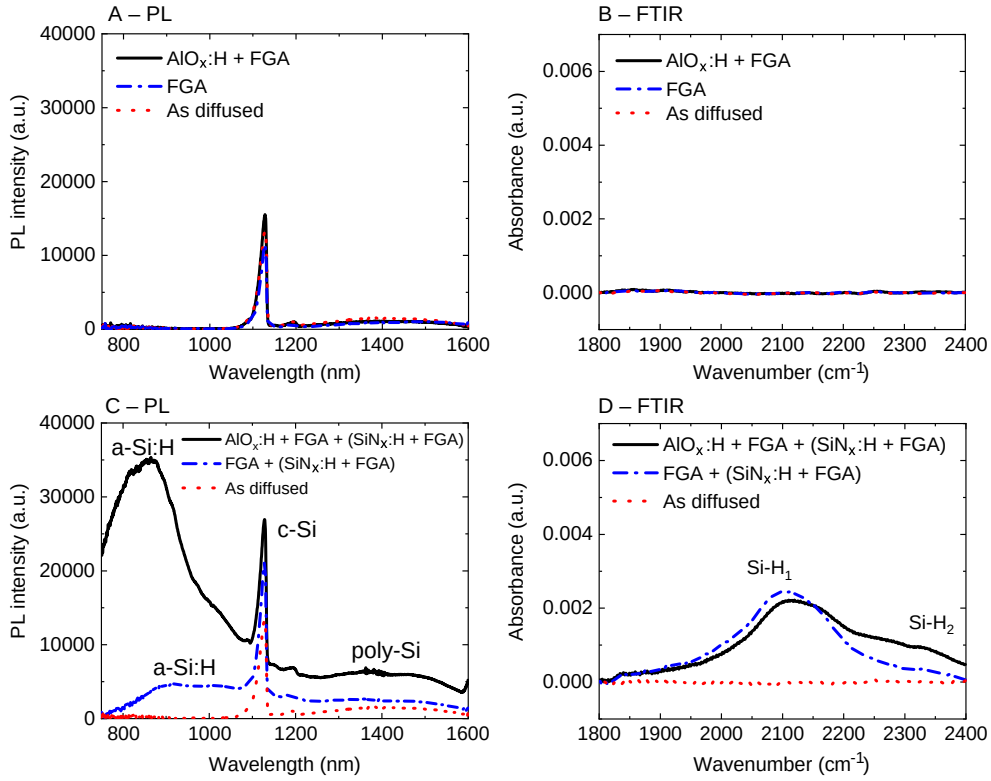

Figure 3. PL spectra captured from the phosphorus-doped poly-Si/SiO_x/c-Si samples after A) plasma-assisted ALD AlO_x:H + FGA hydrogenation and C) the subsequent SiN_x:H + FGA hydrogenation, using the 405 nm excitation laser at 80 K. B,D) Their respective FTIR absorbance spectra in the Si—H wavenumber range of 1800–2400 cm^{-1}. The samples' substrate resistivity is 2 Ω cm.

the poly-Si films or the dangling bonds associated with the a-Si phase.

We continue to assess the Si—H stretching mode at ≈2100 cm^{-1}[25,30,31] from FTIR spectra captured from the sample (Figure 3B). The three spectra (as diffused, after FGA, and after AlO_x:H + FGA) are identical and there is no signal from the Si—H bonds. This is strong evidence that the hydrogenated fraction of the a-Si component inside the poly-Si films was relatively small and below the detection limit of our FTIR system.

In contrast, it is known that after annealing the samples in forming gas in the presence of a SiN_x:H layer the performance of the poly-Si/SiO_x passivating contacts is dramatically improved, compared to the as-diffused case, and the corresponding PL spectra show a clear peak identifiable as a-Si:H.[9] To compare the AlO_x:H + FGA and SiN_x:H + FGA hydrogen treatments,

we continued by capping the already hydrogenated samples (via FGA alone and AlO_x:H + FGA) with SiN_x:H films and subsequently annealed them in forming gas (SiN_x:H + FGA). Figure 1A,B display the τ_{eff} and iV_{oc} values after the second hydrogenation step (i.e., SiN_x:H + FGA). There was a slight reduction in the passivation quality of the samples initially hydrogenated by AlO_x:H + FGA (of both low- and high-resistivity substrates) but a significant improvement of samples initially hydrogenated by FGA only (especially low-resistivity substrates). The surface passivation reduction of the samples with pre-AlO_x:H + FGA after the second hydrogenation step by SiN_x:H + FGA (after having removed the AlO_x:H layer) could be due to two possible reasons. First, the hydrogenated poly-Si films may have been damaged by the plasma from the PECVD SiN_x:H deposition.[32,33] Second, the samples may have been injected with too much hydrogen, which could cause a hydrogen-induced degradation.[34] We can conclude that the former is the main reason for the decreasing passivation quality, as we subsequently injected even more hydrogen by a third hydrogenation step (SiN_x:H + FGA 2) but did not observe any passivation change (Figure 1, SiN_x:H + FGA 2). Despite that, iV_{oc} values were all very high (715–727 mV) after the second hydrogenation step. Note that, using the Kane and Swanson method,[35] we found that all recombination current density J_o values decreased significantly after the different post-treatments, compared to the as-diffused case. This indicates that a large density of defects at the interfaces, either c-Si/SiO_x or poly-Si/SiO_x, was passivated.

Figure 3C shows the PL spectra captured from the samples after the second hydrogenation step (SiN_x:H + FGA) at 80 K. Consistently with the observations in Truong et al.,[9] the PL spectrum captured from the sample with pre-FGA shows clear PL peaks from a-Si:H (800–1000 nm), c-Si (1125 nm), and poly-Si (1300–1500 nm). Compared to the as-diffused sample, the poly-Si PL intensity (FGA + (SiN_x + FGA)) also increases, indicating that some nonradiative defects inside the poly-Si layer have been passivated. Interestingly, the PL spectrum from the sample with pre-AlO_x:H + FGA even shows a much more significant increment in the PL intensities of both a-Si:H and poly-Si (AlO_x:H + FGA + (SiN_x + FGA)). These results suggest that as more hydrogen is injected, more nonradiative defects inside the poly-Si films and their a-Si phase are passivated.

We then verified the presence of hydrogen in the poly-Si films using FTIR measurements, as shown in Figure 3D. Compared to the as-diffused sample, after the SiN_x:H + FGA hydrogenation, the sample with pre-FGA only showed a clear monohydride Si—H_1 peak, whereas the sample with pre-AlO_x:H + FGA displayed both monohydride Si—H_1 and dihydride Si—H_2 peaks, consistent with the literature.[25,30] The presence of a dihydride Si—H_2 mode indicates that more hydrogen was injected into the films and incorporated with a larger amount of a-Si phase.[36] This result further agrees with the captured PL spectra from SiN_x:H + FGA hydrogenated samples, as displayed in Figure 3C.

We continue to evaluate the effects of different hydrogenation treatments on sheet resistance values and dopant concentrations inside the doped poly-Si films. The sheet resistances of the samples before and after the hydrogenation processes, measured by the four-point probe technique, are displayed in **Figure 4**A. The sheet resistance was almost identical after the various treatments. Electrically active phosphorus dopant profiles of the samples before and after the hydrogenation treatments were measured by the ECV technique and are shown in Figure 4B. After the hydrogenation treatment by SiN_x:H + FGA, the active phosphorus concentration in the poly-Si film was slightly reduced (ΔP of about 1–3 × 10^{19} cm^{-3}), despite having a negligible effect on the sheet resistance. This reduction could possibly be a consequence of hydrogenation as hydrogen atoms can associate with some active dopant atoms. Note that, to reduce the measurement uncertainty, the as-diffused and FGA + (SiN_x:H + FGA) profiles were measured on adjacent locations of the same quartered wafer, and so were the AlO_x:H + FGA and AlO_x:H + FGA + (SiN_x:H + FGA) profiles.

Finally, Figure 4C shows SIMS hydrogen profiles inside the doped poly-Si films after the different hydrogen treatments. The oxide location is revealed by a clear peak located ≈60 nm from the surface. After the hydrogen treatments, the profiles showed significant hydrogen in the poly-Si films. Surprisingly, similar hydrogen contents were observed for the AlO_x:H + FGA and FGA + (SiN_x:H + FGA) treated samples, although the former did not show any a-Si:H PL peak (Figure 3A) or any Si—H stretching mode (Figure 3B), whereas the latter did (Figure 3C,D). We hypothesize that the two different capping layers, AlO_x:H and SiN_x:H, could cause different associations of hydrogen in the poly-Si films, as illustrated in Figure 4D. The hydrogen from the AlO_x:H film could be injected into the poly-Si film and form complexes with other species rather than passivate the dangling bonds of the a-Si phase. Meanwhile, the hydrogen atoms from the SiN_x:H film both passivate the a-Si phase and form complexes. Consequently, after the two-step treatment by (AlO_x:H + FGA) + (SiN_x:H + FGA), the hydrogen concentration increases compared to both types of single step (Figure 4C) and the a-Si:H PL and Si–H FTIR peaks also increase significantly. With the two-step treatment, more hydrogen from the second process (SiN_x:H + FGA) is available to passivate the a-Si dangling bonds as other species in the poly-Si film have already formed complexes with the hydrogen from the first process (AlO_x:H + FGA).

In conclusion, we have investigated the mechanisms of various posttreatment techniques of poly-Si/SiO_x passivating contacts, including FGA, AlO_x:H + FGA, and SiN_x:H + FGA. Although all the treatment techniques investigated are effective, there are significant differences between them. For FGA, the performance depends on the substrates' resistivity. The captured PL and FTIR spectra of the samples treated with FGA alone and those of the samples treated with AlO_x:H + FGA are identical to the captured PL and FTIR spectra of the as-diffused sample (no a-Si:H PL peak and no Si-H FTIR peak, respectively). This demonstrates that only a very small amount of the injected hydrogen has been associated with the a-Si phase in the films, albeit a sufficient amount to passivate the interfaces, particularly in the case of AlO_x:H. However, after a subsequent second treatment step (SiN_x:H + FGA), the a-Si:H and Si-H peaks are revealed, demonstrating that hydrogen from the SiN_x:H film can passivate dangling bonds of the a-Si phase more effectively than hydrogen from the AlO_x:H film, even though in this study it did not result in a further improvement of the interfaces. Finally, we have

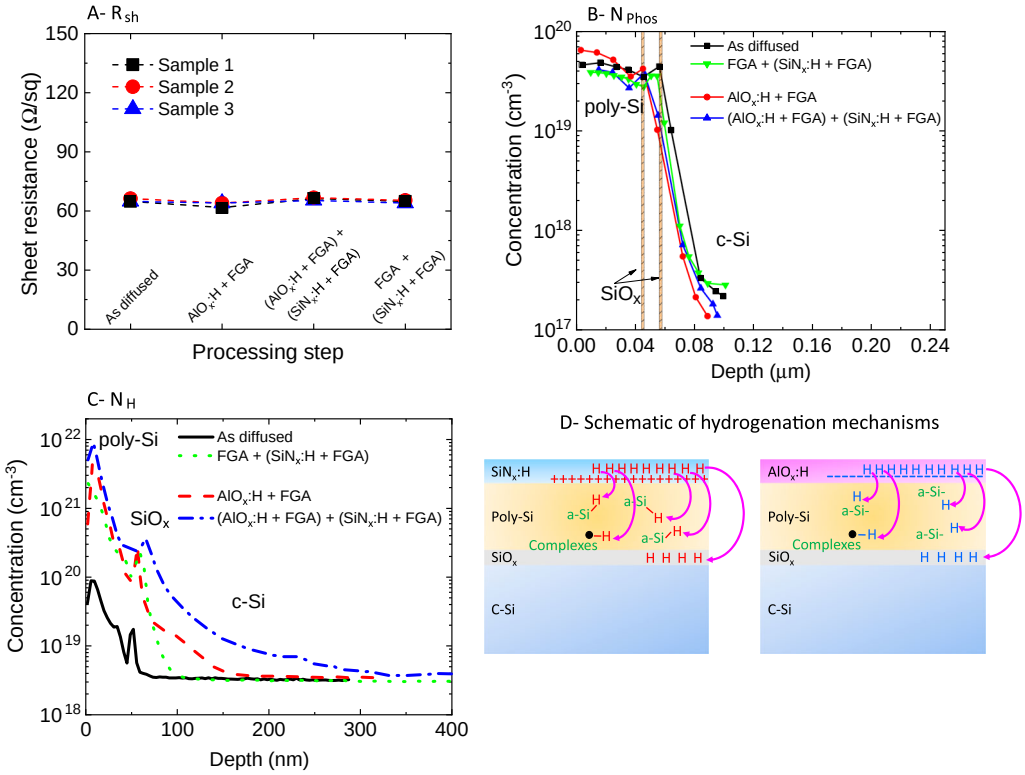

Figure 4. A) Sheet resistances of different samples at various processing steps. B) Electrically active phosphorus dopant concentrations by ECV measurements. C) Hydrogen profiles by SIMS before and after different hydrogenation steps. D) Schematic of the proposed hydrogenation mechanisms from different capping layers. The samples' substrate resistivity was 2 Ω cm. The AlO_x:H films were deposited via the thermally assisted ALD technique.

found that the sheet resistance of the passivating contacts is not affected by the various posttreatment techniques.

Experimental Section

Details of experimental processes are given in Figure 2. The investigated samples were <100> oriented high-quality float-zone n-type c-Si wafers with a thickness of 300 μm and resistivity of either 2 or 100 Ω cm. After a saw-damage etching and cleaning step, all wafers were cleaned by standard RCA 1 and 2 solutions and a layer of silicon oxide (SiO_x) was grown chemically by immersing the c-Si wafers into a 68% nitric acid solution at a temperature of 90 °C for 30 min. The resultant oxide thickness is about 1.3 nm, determined by ellipsometry measurements.[13] The samples were then coated with a layer of hydrogenated amorphous Si (a-Si:H) with a thickness of about 80 nm by a plasma-enhanced chemical vapor deposition (PECVD) system on both sides. They were then subjected to a dopant diffusion process in a quartz tube furnace using $POCl_3$ as a diffusion source to form phosphorus-doped poly-Si films at a temperature of 830 °C. The resultant phosphorus silicate glass (PSG) layers were removed by dipping the samples in a diluted HF solution. Subsequently, some samples continued going through a hydrogen treatment by a 40 nm plasma-assisted or thermal atomic layer deposition (ALD) AlO_x:H film followed by post-FGA at 400 °C for 30 min. After the AlO_x:H layers were removed, 40 nm PECVD SiN_x:H films were deposited on both sides of some samples and they were postannealed in FGA for comparison studies of the hydrogenation methods. All measurements (photoluminescence, PL; quasi-steady-state photoconductance, QSSPC; Fourier transform infrared spectroscopy, FTIR; electrochemical capacitance voltage, ECV; and dynamic secondary ion mass spectrometry, SIMS) were performed after the AlO_x:H or SiN_x:H films (if present) were removed by dipping the samples in a diluted HF solution. We found that removing the dielectric capping layers by this method had no effect on the implied open circuit voltage (iV_{oc}) and the effective minority carrier lifetime (τ_{eff}).

A HORIBA LabRAM system equipped with a confocal microscope was used for steady-state micro-PL spectroscopy measurements. A 405 nm laser light was focused onto the sample surface through a 50× objective lens, yielding a spot diameter of 5 μm. An InGaAs detector with a detection range from 750 to 1600 nm was used to collect the emitted PL signals. All PL measurements were performed at around 80 K using a liquid-nitrogen-cooled THMS600 Linkam stage. A Sinton Instruments WCT-120 contactless photoconductance tester was used to perform τ_{eff} and iV_{oc} measurements.[37–39] FTIR absorbance spectra were recorded in the range 400–4000 cm^{-1} with a resolution of 6 cm^{-1} by a Bruker VERTEX 80v vacuum spectrometer. Dopant profiles in the doped poly-Si films were determined by a Wafer Profiler CVP21 ECV system. A Cameca IMS 7*f* dynamic SIMS system using Cs+ primary ion at 10 kV with the sample at a −5 kV potential for negative secondary ions and an impact energy of 15 kV was used to obtain the hydrogen profiles.

Acknowledgements

This work was supported by the Australian Renewable Energy Agency (ARENA) through Research Grant RND017. The authors acknowledge the facility and technical support from the Department of Electronic Materials Engineering, Research School of Physics & Engineering, ANU College of Science, The Australian National University. H.T.N. acknowledges the fellowship support from the Australian Centre for Advanced Photovoltaics (ACAP). M.T. acknowledges the research support from the Australian Government Research Training Program (RTP) Scholarship.

Conflict of Interest

The authors declare no conflict of interest.

Keywords

aluminum oxide, doped polycrystalline silicon, forming gas anneal, hydrogenation, passivating contacts, silicon nitride

Received: October 27, 2019
Revised: November 18, 2019
Published online:

[1] International Technology Roadmap for Photovoltaic (ITRPV): Results, http://www.itrpv.net/ (accessed: September 2019).
[2] A. Blakers, *IEEE J. Photovoltaics* **2019**, *9*, 629.
[3] M. A. Green, *Prog. Energy* **2019**, *1*, 013001.
[4] F. Haase, C. Hollemann, S. Schäfer, A. Merkle, M. Rienäcker, J. Krügener, R. Brendel, R. Peibst, *Sol. Energy Mater. Sol. Cells* **2018**, *186*, 184.
[5] A. Richter, J. Benick, R. Müller, F. Feldmann, C. Reichel, M. Hermle, S. W. Glunz, *Prog. Photovoltaics Res. Appl.* **2018**, *26*, 579.
[6] D. Yan, S. P. Phang, Y. Wan, C. Samundsett, D. Macdonald, A. Cuevas, *Sol. Energy Mater. Sol. Cells* **2019**, *193*, 80.
[7] M. A. Green, Y. Hishikawa, E. D. Dunlop, D. H. Levi, J. Hohl-Ebinger, M. Yoshita, A. W. Y. Ho-Baillie, *Prog. Photovoltaics Res. Appl.* **2019**, *27*, 3.
[8] F. Feldmann, M. Bivour, C. Reichel, H. Steinkemper, M. Hermle, S. W. Glunz, *Sol. Energy Mater. Sol. Cells* **2014**, *131*, 46.
[9] T. N. Truong, D. Yan, C. Samundsett, R. Basnet, M. Tebyetekerwa, L. Li, F. Kremer, A. Cuevas, D. Macdonald, H. T. Nguyen, *ACS Appl. Mater. Interfaces* **2019**, *11*, 5554.
[10] J. I. Pankove, D. E. Carlson, *Appl. Phys. Lett.* **1977**, *31*, 450.
[11] J. Dresner, in *Semiconductors and Semimetals*, Academic Press, Inc., London **1984**, pp. 193–205, Ch. 5.
[12] J. I. Pankove, M. A. Lampert, M. L. Tarng, *Appl. Phys. Lett.* **1978**, *32*, 439.
[13] D. Yan, A. Cuevas, J. Bullock, Y. Wan, C. Samundsett, *Sol. Energy Mater. Sol. Cells* **2015**, *142*, 75.
[14] D. Yan, A. Cuevas, Y. Wan, J. Bullock, *Sol. Energy Mater. Sol. Cells* **2016**, *152*, 73.
[15] Z. Zhang, M. Liao, Y. Huang, X. Guo, Q. Yang, Z. Wang, T. Gao, C. Shou, Y. Zeng, B. Yan, J. Ye, *Sol. RRL* **2019**, *3*, 1900105.
[16] B. Hoex, M. C. M. van de Sanden, J. Schmidt, R. Brendel, W. M. M. Kessels, *Phys. Status Solidi RRL* **2012**, *6*, 4.
[17] B. Hoex, M. Bosman, N. Nandakumar, W. M. M. Kessels, *Phys. Status Solidi RRL* **2013**, *7*, 937.
[18] G. Dingemans, W. M. M. Kessels, *J. Vac. Sci. Technol., A* **2012**, *30*, 040802.
[19] A. Richter, J. Benick, M. Hermle, *IEEE J. Photovoltaics* **2013**, *3*, 236.
[20] A. To, S. Tahir, A. Garavaglia, W. M. Li, X. Li, B. Hoex, *IEEE J. Photovoltaics* **2017**, *7*, 1528.
[21] B. Hallam, D. Chen, M. Kim, B. Stefani, B. Hoex, M. Abbott, S. Wenham, *Phys. Status Solidi A* **2017**, *214*, 1700305.
[22] S. Wilking, S. Ebert, A. Herguth, G. Hahn, *J. Appl. Phys.* **2013**, *114*, 194512.
[23] Y. Wan, K. R. McIntosh, A. F. Thomson, A. Cuevas, *Appl. Phys. Lett.* **2015**, *106*, 1.
[24] M. Schnabel, B. W. H. van de Loo, W. Nemeth, B. Macco, P. Stradins, W. M. M. Kessels, D. L. Young, *Appl. Phys. Lett.* **2018**, *112*, 203901.
[25] M. Lozac'h, S. Nunomura, H. Sai, K. Matsubara, *Sol. Energy Mater. Sol. Cells* **2018**, *185*, 8.
[26] M. Lozac'h, S. Nunomura, H. Umishio, T. Matsui, K. Matsubara, *Jpn. J. Appl. Phys.* **2019**, *58*, 050915.
[27] H. T. Nguyen, F. E. Rougieux, B. Mitchell, D. Macdonald, *J. Appl. Phys.* **2014**, *115*, 43710.
[28] H. T. Nguyen, F. E. Rougieux, D. Yan, Y. Wan, S. Mokkapati, S. M. De Nicolas, J. P. Seif, S. De Wolf, D. MacDonald, *Sol. Energy Mater. Sol. Cells* **2016**, *145*, 403.
[29] H. T. Nguyen, A. Liu, D. Yan, H. Guthrey, T. N. Truong, M. Tebyetekerwa, Z. Li, Z. Li, M. M. Al-Jassim, A. Cuevas, D. Macdonald, *ACS Appl. Energy Mater.* **2018**, *1*, 6619.
[30] M. Saß, A. Annen, W. Jacob, *J. Appl. Phys.* **1997**, *82*, 1905.
[31] B. Hallam, B. Tjahjono, S. Wenham, *Sol. Energy Mater. Sol. Cells* **2012**, *96*, 173.
[32] S. Jan, K. Mark, C. Andrés, *Semicond. Sci. Technol.* **2001**, *16*, 164.
[33] J. Shi, Z. C. Holman, in *2017 IEEE 44th Photovoltaic Specialist Conf. (PVSC)*, IEEE, Piscataway, New Jersy, USA **2017**, pp. 1820–1823.
[34] A. C. N. Wenham, S. Wenham, R. Chen, C. Chan, D. Chen, B. Hallam, D. Payne, T. Fung, M. Kim, S. Liu, S. Wang, K. Kim, A. Samadi, C. Sen, C. Vargas, U. Varshney, B. V. Stefani, P. Hamer, G. Bourret-Sicotte, N. Nampalli, Z. Hameiri, C. Chong, M. Abbott, in *2018 IEEE 7th World Conf. Photovolt. Energy Conversion, WCPEC 2018 – A Jt. Conf. 45th IEEE PVSC, 28th PVSEC 34th EU PVSEC*, **2018**, pp. 1–8.
[35] D. E. Kane, R. M. Swanson, in *18th IEEE Photovoltaic Specialists Conf.*, IEEE, Piscataway, New Jersy, USA **1985**, pp. 578–583.
[36] K. Gotoh, M. Wilde, S. Kato, S. Ogura, Y. Kurokawa, K. Fukutani, N. Usami, *AIP Adv.* **2019**, *9*, 075115.
[37] A. Cuevas, D. Macdonald, *Sol. Energy* **2004**, *76*, 255.
[38] A. Cuevas, R. A. Sinton, M. Kerr, D. Macdonald, H. Mäckel, *Sol. Energy Mater. Sol. Cells* **2002**, *71*, 295.
[39] A. Cuevas, *Sol. Energy Mater. Sol. Cells* **1999**, *57*, 277.